MIC2021
21st Machining Innovations Conference for Aerospace Industry

Proceedings are available on SSRN: www.ssrn.com

SSRN Proceedings Hosted on SSRN.com

MIC Procedia (2021) 041–049

21st Machining Innovations Conference for Aerospace Industry 2021 (MIC 2021), December 1st and 2nd 2021, Hannover, Germany

Investigations on the Impact of Additively Manufactured Coolant Channels and Outlet Nozzles on Free Jet and Jet Forces in High-Pressure Cutting Fluid Supply

T. Kelliger[a,*], H.Liu[a], D. Schraknepper[a], T. Bergs[a,b]

[a] *Laboratory for Machine Tools and Production Engineering (WZL) of RWTH Aachen University, Germany*
[b] *Fraunhofer Institute for Production Technology (IPT), Germany*

* Corresponding author. Tel.: +49 241 80 20523; *E-mail address:* T.Kelliger@wzl.rwth-aachen.de

Abstract

The focused high-pressure cutting fluid supply into the contact zone between the rake face of a cutting tool and the emerging chip helps to increase tool life and to improve chip evacuation. Moreover, the productivity of the cutting process can be increased due to higher applicable cutting parameters. Traditionally manufactured milling tools feature drilled coolant channels with sharp intersections, causing pressure losses between channel inlets and outlets. Moreover, the resulting turbulences lead to an undesirable expansion of the cutting fluid free jet. Additive manufacturing technologies, such as Laser Powder Bed Fusion (LPBF), allow an enhanced freedom of design. Thus, the technology enables the manufacturing of cutting tools with flow-optimized coolant channels that feature smooth radii transitions and nozzles specifically designed for the application. In this paper, a novel test bench for analyzing the cutting fluid free jet and jet forces under high-pressure cutting fluid supply with additively manufactured coolant channels with different channel geometries as well as different outlet nozzles is presented. Furthermore, the impact of post-processing the inner surfaces by means of abrasive flow machining is investigated. The results are compared with computational fluid dynamics (CFD) simulations. The investigations show that flow losses in additively manufactured and geometry-improved coolant channels can be decreased in comparison to traditionally drilled channels. Further, the fluid free jet expansion can be reduced depending on the nozzle design. The cooling and lubrication can be enhanced due to a more focused cutting fluid supply and higher flow velocities.

Keywords: cutting tool; coolant channel; high-pressure cutting fluid supply; flow optimization; computational fluid dynamics; additive manufacturing; Laser Powder Bed Fusion

1. Introduction

In machining hard to cut materials, an increase in tool life as well as in productivity can significantly reduce ecological and economical costs of the tools and thus of the products to be manufactured [1]. Both the tool life and the productivity of the cutting process can be expanded by targeted cutting fluid supply into the contact zone between the rake face of the cutting tool and the emerging chip [2, 3]. The focused high-pressure cutting fluid supply helps not only to reduce friction in the cutting zone but also to improve heat dissipation from the cutting tool and machined workpiece as well as chip evacuation [4–6].

Investigations by Klocke et al. [7] indicated a significant increase in tool life (up to 60 %) and decrease in tool wear for milling tools with a focused high-pressure cutting fluid supply. Results showed a dependency of the impact point of the cutting fluid free jet onto the cutting insert on the tool wear. In addition,

a strong dependency of the machined material on the optimal impact point was detected. For 42CrMo4 Q+T, a cutting fluid supply with two outlet nozzles directed towards the corner and the rake face of the insert was found to reduce tool wear. For TiAl6V4, the lowest tool wear was detected for a cutting fluid supply with one nozzle only directed towards the insert's corner.

Manufacturing the coolant channels for material-specific cutting tools is possible by conventional, subtractive manufacturing technologies such as drilling and electrochemical or electrical discharge machining [8]. However, it is very time-consuming and expensive to manufacture complex channel sections in a tool such as an indexable milling tool with cutting inserts in multiple rows, e.g. shell end mills. Furthermore, sharp intersections between channels lead to an increase in flow losses due to turbulences and friction within the cutting fluid stream, thus lowering the cooling and lubrication effect [9].

To overcome these drawbacks, additive manufacturing (AM) techniques such as Laser Powder Bed Fusion (LPBF) can be used to manufacture indexable cutting tools in very few process steps with flow-optimized coolant channels as well as a focused and material-adapted cutting fluid supply through individual outlet nozzle design.

Lakner at al. [10] proved the potential of AM milling tools for cutting of AISI 4140+QT (42CrMo4+QT) material. With the AM tool, tool wear was reduced and feed travel path was increased by 67 % compared to a conventional tool. The AM tool contained a combination of a round and an L-shaped outlet nozzle directed towards each cutting insert, guaranteeing a wide-spread cutting fluid supply on the rake face.

So far, the design of these AM tools has not been completely based on a thorough scientific methodology. Research regarding additively manufactured coolant channels focused mainly on tools for forming and injection molding or other components for heat exchange with conformal cooling, not taking into account additively manufactured outlet nozzles and geometric boundaries found in indexable milling tools [11–15]. In order to build the basis for valid design guidelines, the impact of additively manufactured (LPBF process) coolant channels and outlet nozzles on flow losses, jet forces and the free jet characteristics were investigated in this paper. Channel and nozzle geometry were designed based on computational fluid dynamics (CFD) analysis taking into account the freedom of design of the LPBF process.

2. Experimental setup and methodology

2.1. Experimental approach

The objective of the presented investigations was to understand the impact of channel and nozzle geometry as well as post-processing of the inner surface by abrasive flow machining of additively manufactured coolant channels on the cutting fluid stream and free jet. A low-loss fluid supply as well as a directed free jet can help to improve the efficiency of the overall supply system and thus lowering energy consumption and increasing the fluid energy reaching the cutting zone.

The influence of channel and nozzle design were investigated separately. Several parameters shown in Table 1 were varied and different values measured while varying the cutting fluid supply pressure between p = 70 bar and 150 bar.

Table 1. Experimental Scope

CHANNEL		NOZZLE	
Varied parameters	**Measurand**	**Varied parameters**	**Measurand**
Cross-section geometry	Volume flow	Geometry	Volume flow
Cross-sectional area			Total jet force
Transition radius	Total jet force	Cross-sectional area	Jet force distribution
Surface post-processing			Free jet

All experiments were performed on a lathe of the type DMG MORI NEF 600. The cutting fluid BLASER Swisslube Vasco TP 519 (8 %) was supplied by a high-pressure unit of the type Chip Blaster WVHP6-60 independently from the machine internal supply system.

2.2. Experimental setup, evaluation method and test specimens

The developed test bench installed inside the lathe was based on previous investigations by Sangermann [6] and is presented in Fig. 1. The volume flow was measured using a sensor of the type PKP Prozesstechnik GmbH DV04.7 which was installed within the supply pipeline. For all supply pressure stages, a mean value of three measurement values was calculated. The test specimen was mounted on a device clamped in the tool turret with the outlet pointed perpendicular to a sensing element mounted on a dynamometer of the type KISTLER 9119AA2. For measuring the total jet force F_{jet}, an impact plate was mounted onto the dynamometer. In order to measure the jet force distribution F_z, a thin blade was mounted between two bolts. With the help of a shielding metal mounted outside the flow of forces of the dynamometer, only the jet force impacting the blade (sensing element) was measured. Moving the test specimen up and down, a force distribution could be illustrated for rotationally symmetric free jets. Total jet force and force distribution were measured in different distances s between the nozzle outlet and the impingement point of the jet. The free jet characteristic was observed qualitatively using a conventional digital camera positioned at the observation window outside the machine.

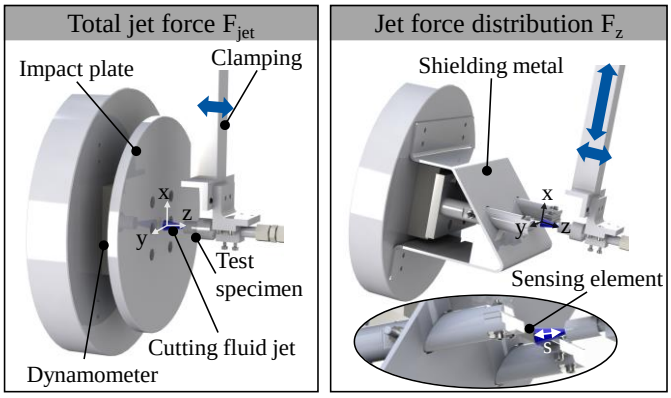

Fig. 1. Test bench for the investigation on additively manufactured coolant channels and outlet nozzles

Measuring jet forces can help to validate the CFD-simulation especially for the simulation of the emerging free jet. In theory, the total jet force can be related to the volume flow Q_{th} and the dynamic pressure p_{dyn} following the equation (with the fluid velocity v_{th}):

$$F_{jet,th} = \rho \cdot \alpha \cdot Q_{th} \cdot v_{th} = \rho \cdot \alpha \cdot Q_{th} \cdot \sqrt{\frac{2 \cdot p_{dyn}}{\rho}} \quad (1)$$

Thus, the total jet force is proportional to the volume flow Q_{th} and to the root of the dynamic pressure p_{dyn}. The flow coefficient α describes the relation between the measured volume flow $Q_{measured}$ and the theoretical volume flow Q_{th} [6] (with the cross-sectional area A_{th}):

$$\alpha = \frac{Q_{measured}}{Q_{th}} = \frac{Q_{measured}}{A_{th} \cdot v_{th}} \quad (2)$$

All test specimens were built on a LPBF machine Aconity MIDI at Fraunhofer Institute for Laser Technology, Germany. The specimens were built from a newly developed bainitic steel alloy powder "Bainidur AM" provided by Deutsche Edelstahlwerke Specialty Steel GmbH & Co. KG and partly post-processed via abrasive flow machining by 4MI GmbH. The relative density of the manufactured components was > 99.9 %. At the time of the experiments, LPBF contour, up- and down-skin parameters were not yet optimized for a minimum surface roughness and maximum geometrical accuracy. The specimen geometries and design of experiments for channel and nozzle tests are shown in Fig. 2 and Fig. 3.

For the investigation of the coolant channel geometry, several specimens with a channel transition of 90° and a total length between 33.7 mm and 38 mm were designed and manufactured. Channel diameters were varied between $d_{channel}$ = 1.4 mm and 3 mm and transition radii r = 0 mm, 5 mm and 10 mm examined. Furthermore, circular, triangular and rectangular cross section geometries with a comparable cross-sectional area were investigated. In addition, post-processed channels were compared with as-built structures (in the following $d_{channel}$ is used for the description of the channel size).

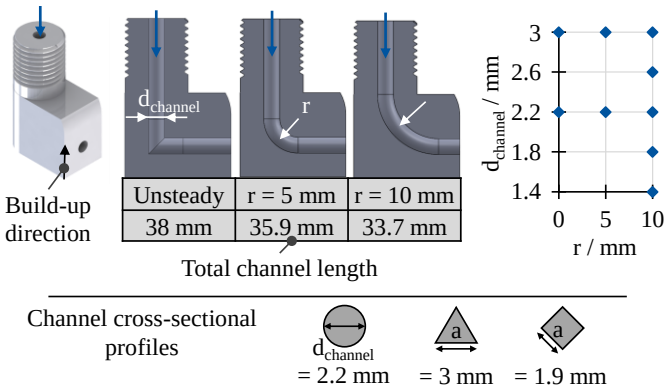

Fig. 2. Specimen geometries and design of experiments for the investigation of coolant channels

Six different outlet nozzle geometries were tested in the as-built state (see Fig. 3). The inlet channel diameter was constant and cylindrical with $d_{channel}$ = 3 mm for all nozzle specimens. The outlet geometry varied between round (discontinuous, tapered, convex-concave shape), triangular, rectangular and L-formed. All specimens were built up in vertical direction to the building platform of the LPBF machine to avoid varying surface roughness influencing and deflecting the fluid flow. Besides the geometrical form, the aspect ratio between inlet and outlet cross-sectional area was modified. Only nozzles with the same outlet cross-sectional area A_{nozzle} (in the following d_{nozzle} is used for the description of the nozzle size) can be directly compared when analyzing the volume flow Q following Bernoulli:

$$Q = v \cdot A_{nozzle} \quad (3)$$

For the convex-concave nozzle geometry, design guidelines from [16, 17] were taken into account. For all non-circular nozzle outlet geometries, smooth guide trajectories were applied in the CAD-software SolidWorks 2019 for a continuous transition between circular inlet channel and angular outlet.

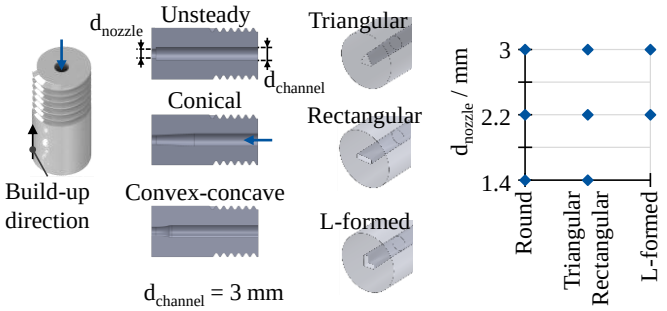

Fig. 3. Specimen geometries and design of experiments for the investigation of outlet nozzles

3. Results and Discussion

3.1. CFD Analysis

The afterwards experimentally studied channel specimens were first analyzed numerically using CFD simulation. For channel calculations, a one-phase κ-ω-SST turbulence model was used as it provides a high accuracy in near-wall areas as well as in the free stream [18, 19]. The cutting fluid, a water-based emulsion, was simplified modelled as water, respecting its main characteristics. A fully turbulent flow was assumed ($Re \geq 4000$) [20]. Inlet pressures p = 50 bar and 150 bar as well as surface roughness Rz = 5 µm and 200 µm were predefined. In Fig. 5, the resulting velocity profiles for a circular cross section $d_{channel}$ = 2.2 mm and different transition radii as well as a triangular cross section with side length a = 3 mm and a rectangular cross section with a = 1.9 mm for p = 150 bar are illustrated exemplary.

As the inlet pressure is equal for every specimen, the volume flow Q indicates the losses within the channel through turbulences and wall friction. The results illustrate the great impact of a smooth intersection between two perpendicular coolant channels on flow losses as well as velocity profile. The volume flow was increased by +27 % for a transition radius of 5 mm compared to a sharp intersection for both pressure levels 50 bar and 150 bar. Doubling the transition radius from 5 mm to 10 mm did not have a big impact on flow losses (+3 %) but led to an improved homogeneity of the velocity profile at the channels outlet. In constricted space such as an indexable milling tool with 50 mm outer diameter, the radius thus can be

designed smaller without significant additional energy losses of the fluid jet. The influence of post-processing the coolant channel was significant especially for smooth transition radii. For the reduced surface roughness Rz = 5 µm, the flow rate was increased between 14 % and 18 % for radii 5 mm and 10 mm compared to Rz = 200 µm.

The sectional views A-A for different cross-sectional geometries clearly show the secondary flow in all of the simulated channel designs after the transition. The triangular and rectangular cross section lead to velocity reductions in the sharp corners und thus to a more inhomogeneous velocity profile. As the friction factor as well as the total pressure losses depend on the hydraulic diameter (d_h = 1.7 mm for the triangular and d_h = 1.9 mm for the rectangular cross section compared to d_h = $d_{channel}$ = 2.2 mm for the circular profile), the loss of flow increases for the non-circular profiles due to the lower hydraulic diameter (between -3 % and -8 % for Rz = 200 µm) [20].

3.2. LPBF process-related channel characteristics

The as-built test samples showed significant deviations between the nominal channel diameter and cross-sectional area and the real manufactured part which were measured by optical light microscopy (Fig. 4).

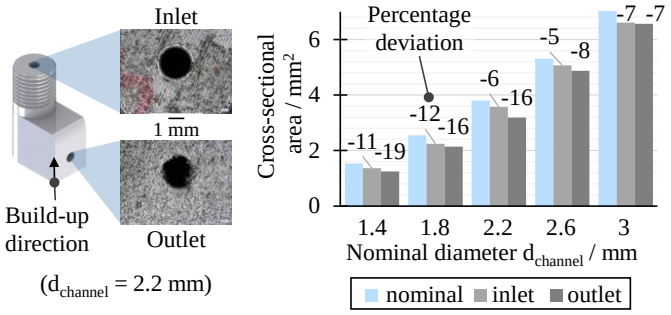

Fig. 4. Geometrical accuracy for circular channels

Depending on the build-up direction and the nominal diameter, the deviation in the cross-sectional area was between -19 % and -5 %, which is in accordance with results obtained by [14]. The horizontal part of the channel at the outlet showed powder adhesions and higher geometrical irregularities compared to the vertical part of the channel at the inlet. This can be explained by the stair-stepping effect as well as collapsing overhang regions, which were not stabilized by support structures.

The surface roughness was measured optically with a microscope Alicona Infinite Focus in eight sliced test specimens of different channel diameters between $d_{channel}$ = 1.4 mm and 3 mm. The vertical part of the channel showed a roughness average of Ra = 11 µm (standard deviation SD = 2 µm) and a mean roughness depth of Rz = 79 µm (SD = 20 µm). For the horizontal part of the coolant channels, Ra = 15 µm (SD = 3 µm) and Rz = 96 µm (SD = 23 µm) was measured.

3.3. Channel Design

Because of the discrepancy between theoretical and measured diameters, a direct comparison between analytically or numerically calculated and measured loss of flow appears inconclusive. Therefore, the measured volume flow was related to the measured cross-sectional area, simplified calculating the fluid velocity v:

$$v = \frac{Q_{measured}}{A_{measured}} \tag{4}$$

For a direct comparison of the efficiency of the channel design, the flow coefficient α was modified taking into account the real, measured cross-sectional area:

$$\alpha' = \frac{Q_{measured}}{A_{measured} \cdot v_{th}} = \frac{Q_{measured}}{A_{measured} \cdot \sqrt{\frac{2 \cdot p_{dyn}}{\rho}}} \tag{5}$$

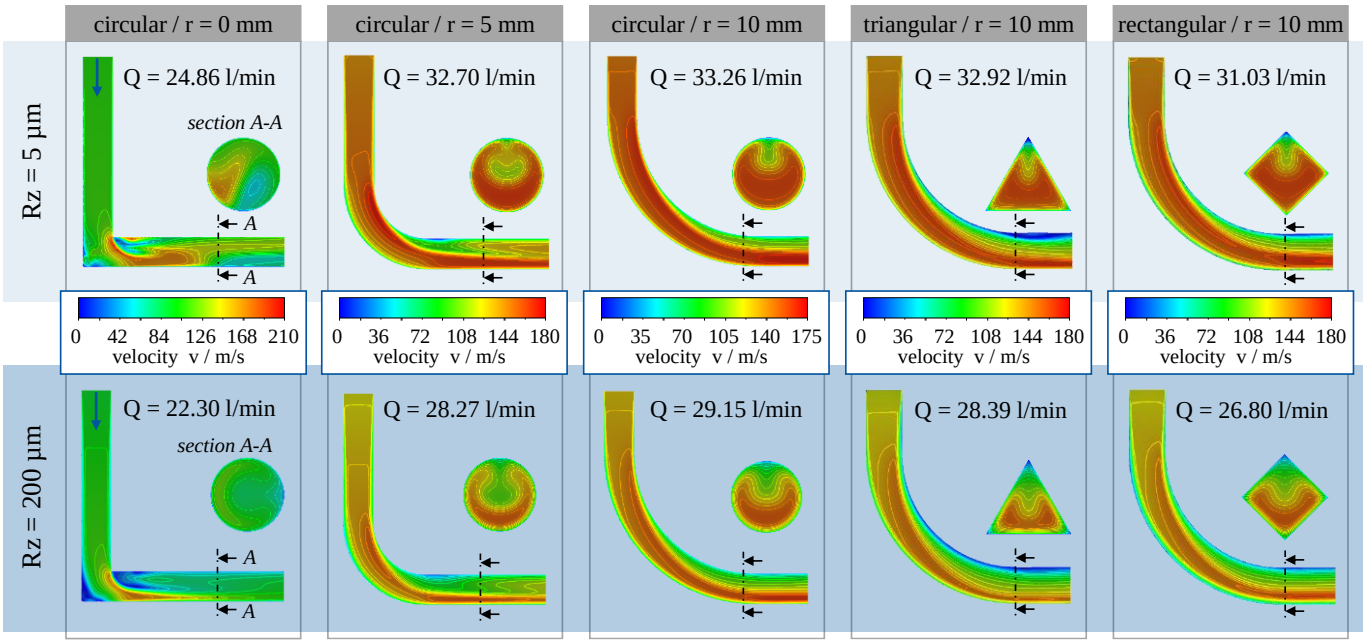

Fig. 5. Velocity profiles obtained from CFD analysis of coolant channels with circular cross section for different transition radii r and with different cross-sectional geometries for different surface roughness Rz (p = 150 bar, $d_{channel}$ = 2.2 mm)

In Fig. 6, the results for different transition radii for channel diameters 2.2 mm and 3 mm are shown. Comparing the average change in volume flow for all pressure levels between r = 0 mm and 5 mm, it increased by 7 % for $d_{channel}$ = 2.2 mm and by 18 % for $d_{channel}$ = 3 mm. For bigger cross-sectional areas, the influence of the transition radius on the loss of flow increases relative to the channels diameter and to the surface roughness. The unaffected area proportion of the fluid cross-section not being affected by the surface roughness increases.

The change in volume flow between 5 mm and 10 mm radius had a relatively small impact on the total losses compared to the change between 0 mm and 5 mm. Thus, in the geometrical boundaries of the real milling tool, lengthening the coolant channel for a bigger transition radius should be avoided, as a small intersection radius reduces losses more effectively.

The average flow coefficient α' was < 0.5 for all pressure levels. This is due to the unconsidered pressure losses within the supply system after the pressure measurement that could not be detected with the presented experimental setup. Therefore, all results must be compared relative to each other.

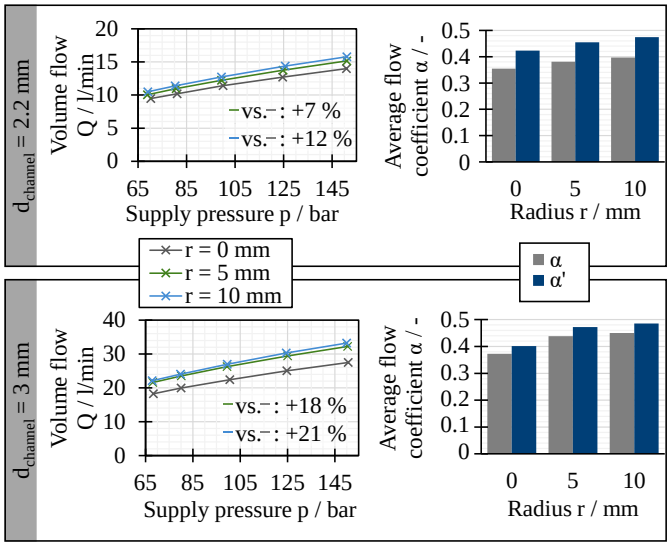

Fig. 6. Volume flow and flow coefficient for different transition radii for circular channel cross-section (as-built state)

Comparing different channel diameters, no significant differences in loss of flow were detected for $d_{channel} \geq 2.2$ mm where the calculated fluid velocity and α' were comparable (see Fig. 7). The results can be explained by the decreasing influence of the surface roughness for bigger cross-sectional areas as the proportion of the fluid volume being affected by the roughness peaks decreases.

A triangular channel cross section can help to improve the geometrical accuracy and surface roughness especially when the channel is built in horizontal direction to the build-up direction (see Fig. 8). Thus, it provided the lowest losses compared to circular and rectangular profiles with the same cross-sectional area, even though the simulation predicted higher turbulences and stagnation regions in the corners as stated in chapter 3.1. Although the wetted perimeter and thus the overflowed channel surface was smaller for the rectangular profile than for the triangular cross section (nominal perimeter P = 7.8 mm for rectangular profile vs. P = 8.9 mm for triangular profile), the rectangular profile cannot be recommended as the flow losses increase due to bigger stagnation regions in the corners of the cross-sectional profile (see Fig. 5).

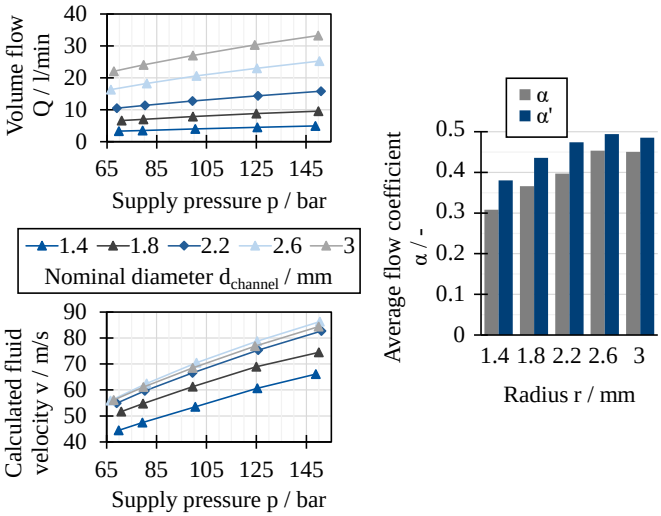

Fig. 7. Volume flow, fluid velocity and flow coefficient for different channel diameters for circular channel cross-section (r = 10 mm, as-built state)

Applying the triangular channel profile to a milling tool with a curved channel pathway within the geometrical boundaries can become difficult, as the sides of the triangle must be orientated taking into account the build-up direction. Avoiding overhang areas can lead to a twist in the channel, which can affect the flow characteristics.

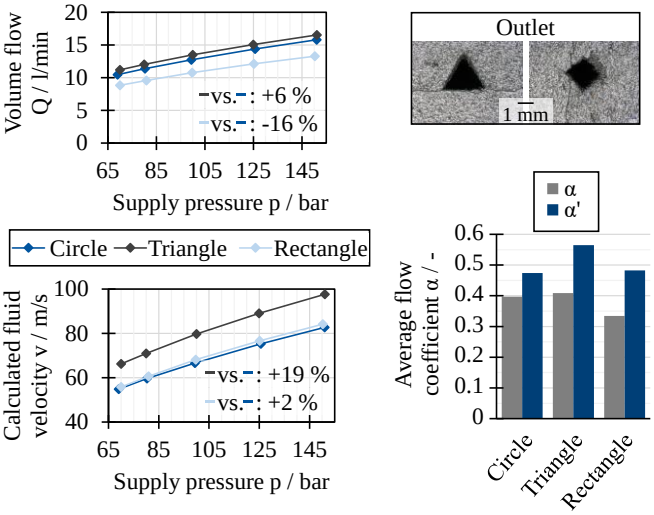

Fig. 8. Volume flow, fluid velocity and flow coefficient for different cross-sectional profiles ($d_{channel}$ = 2.2 mm, r = 10 mm, as-built state)

Circular channel profiles can be improved regarding the surface roughness applying abrasive flow machining. Specimens $d_{channel}$ = 2.2 mm and r = 10 mm were post-processed with three different parameters *P1-P3* (see Fig. 9). In a first step, parameters causing a high material erosion were applied. The process led to a significant expansion of the channel diameter depending on the applied parameters but also to a reduced surface roughness (Ra = 2.4 µm, Rz = 15.1 µm).

Thus, the volume flow increased up to 83 % compared to the as-built specimen. Parameter *P2* led to an increase in calculated fluid velocity of 12 % compared to the as-build channel. It can be stated that abrasive flow machining of the inner channels helps to lower the losses caused by surface roughness. During the design process, the expansion of the cross-section has to be taken into account for a defined dimensioning of the cutting fluid volume flow.

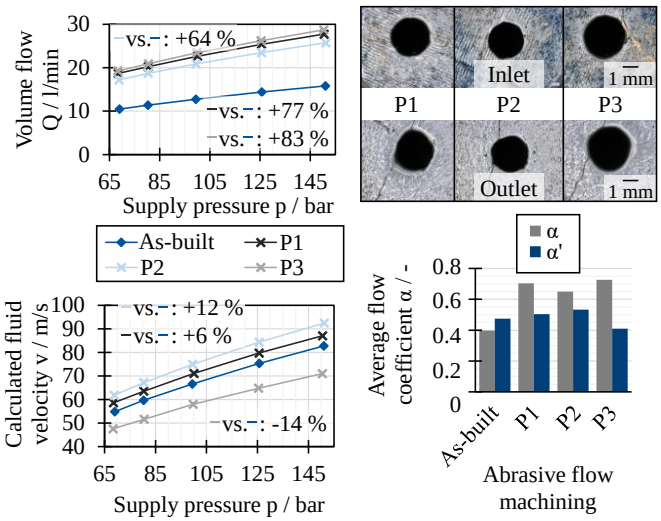

Fig. 9. Geometrical accuracy, flow velocity and flow coefficient for post-processed coolant channels ($d_{channel}$ = 2.2 mm)

The total fluid jet force signal was captured during the whole spraying period. The mean value was calculated taking the last five seconds of the signal into account (see Fig. 10). The jet forces did not decrease for higher distances *s*, thus indicating a negligible influence of the air resistance and entrainment on the free jet energy. The relative comparison of the forces for different radii, diameters and profiles confirm the volume flow measurements.

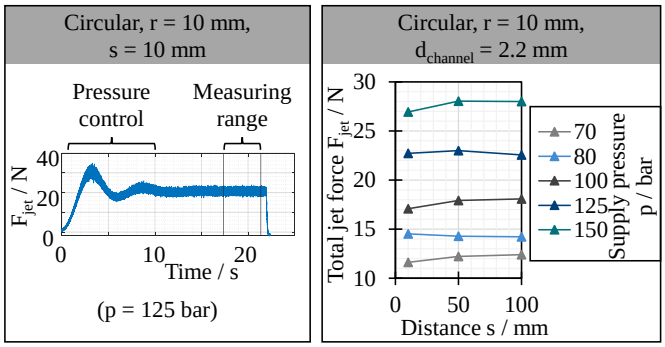

Fig. 10. Analysis of total jet force signal for channel design

3.4. Nozzle Design

Regarding the outlet nozzle test specimens, differences in loss of flow between different nozzle geometries were small (see Fig. 11). A steady change in cross-section led to an increased flow rate of 5 % compared to the unsteady nozzle (d_{nozzle} = 2.2 mm). The change from a circular to an angular cross-section did not result in bigger losses. Comparing different nozzle diameters, the measured losses got bigger for smaller diameters which can be explained by the higher area percentage overflowed by the cutting fluid. The differences of the calculated fluid velocity were slightly higher due to the differences in the measured cross-sectional area. Thus, the rectangular and triangular nozzles appear to cause the lowest losses. For a more informative conclusion, the free jet characteristics for different nozzle geometries were observed.

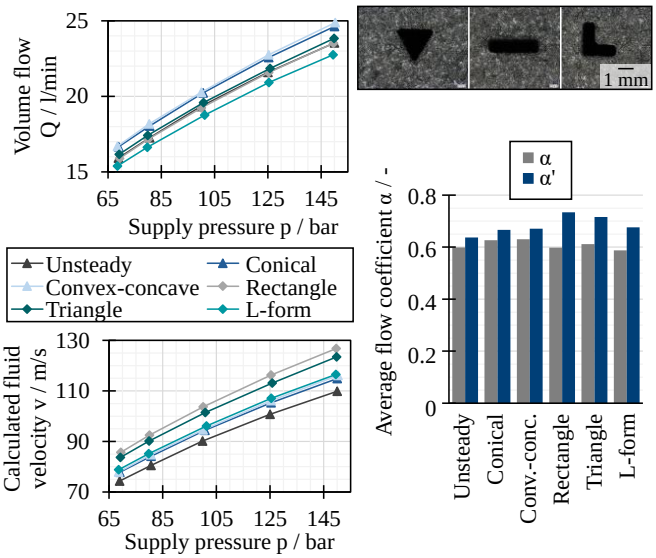

Fig. 11. Volume flow, fluid velocity and flow coefficient for different outlet nozzle geometries (d_{nozzle} = 2.2 mm, as-built state)

In order to characterize the free jet, the measured force signal is plotted against the covered distance in x-direction for different distances *s* between nozzle outlet and sensing element (see Fig. 12). The test specimen was moved along the *x*-direction over the thin side of the blade introduced in chapter 2.2 with a constant feed rate of v_x = 50 m/min. This allowed the calculation of the traveled distance. The feed motion was repeated once with the specimen moving in the same *x*-direction (measuring range 1 and 2). The thin peak halfway in the signal results from the fast movement of the specimen back to the start position in *x*-direction as the fluid stream was kept constant during the whole measurement. The jet diameter was calculated from the signal points where the force F_z reaches 5 % of the maximum force $F_{z,max}$ as described in [21]. Distances between *s* = 5 mm and 50 mm were measured. Even though the distances between nozzle outlet and impingement point of the cutting fluid do normally not exceed 20 mm in most cutting tool applications, the measurement of higher distances can help to validate the results obtained in CFD simulations of the free jet and to better understand the fluid free jet expansion.

Furthermore, the video images were analyzed using a simple image processing based on difference images before and during fluid supply, developed and described in [22]. The processed images could then be correlated to the obtained force signals.

As can be seen in Fig. 12, the maximum force $F_{z,max}$ decreased for higher distances *s* while the force signal widened along the *x*-direction, resulting in an increased jet diameter d_{jet}.

The jet expansion, quantitatively expressed by the jet diameter d_{jet}, appears to increase nearly linear along the distance *s* (see Fig. 13). The fluid supply pressure did not affect the jet expansion in the range *p* = 70 bar to 150 bar. These results are in contrast to [6], where a significant increase in jet expansion was measured for higher supply pressures for a

circular nozzle with d_{nozzle} = 2 mm. As a significant jet expansion for higher supply pressures was also not visible in the video images, the differences cannot be traced back to errors in the experimental setup. As stated above, the real pressure at the nozzle entrance was unknown due to the experimental setup. The flow coefficients were not higher than ≈ 0.75, indicating a pressure loss in the supply system which might explain the differences.

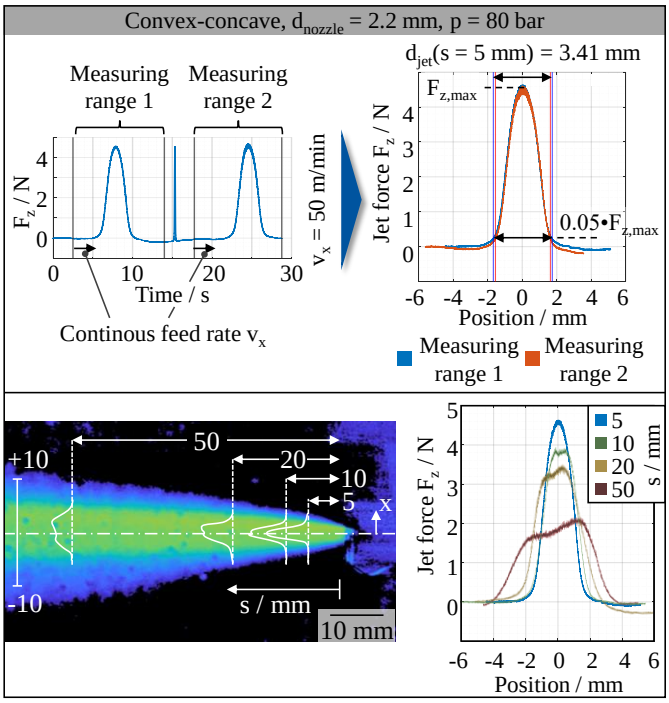

Fig. 12. Evaluation method for the observation of the fluid free jet based on [6, 22]

The maximum force $F_{z,max}$ decreased with higher distance s, which can be explained by the more extensive fluid energy distribution at higher distances.

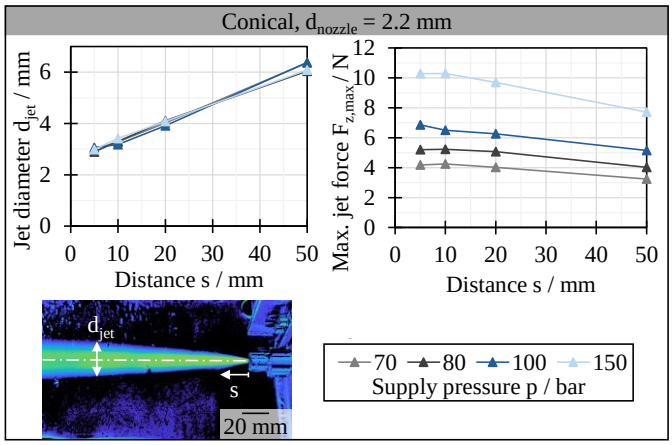

Fig. 13. Jet expansion depending on distance s and supply pressure p (exemplary for conical nozzle geometry)

Comparing different circular nozzle geometries, the unsteady nozzle caused higher losses than the conical nozzle which resulted in lower maximum jet forces and higher jet expansion for small distances s (see Fig. 14). For the conical nozzle, the jet expansion for small distances up to s = 20 mm appeared negligible, also visible in a dense colour distribution in the processed video images. The convex-concave nozzle generated an inhomogeneous jet profile which led to a higher jet expansion and an irregular energy distribution especially for larger distances s. Even though this nozzle type in theory should lead to the lowest losses and best jet profile, it cannot be recommended based on the experimental results. The inaccuracies and powder adhesions of the LPBF-process cause undefined fluid deflections, which can be reduced by an extended change in cross-section.

For the force measurement, the non-rotationally symmetric nozzles were clamped in two positions with a 90° rotation relative to the sensing element (see Fig. 14). The triangular nozzle, in theory helping to decrease the jet expansion, did not generate a more focused free jet profile. However, in the video images, a deflection of the whole jet to the axis of symmetry of the nozzle could be observed for d_{nozzle} = 2.2 mm. Thus, a secure prediction of the jet impingement point on the chip or cutting tool cannot be guaranteed. For d_{nozzle} = 3 mm, no smaller jet expansion was observed comparing the round and the triangular nozzle.

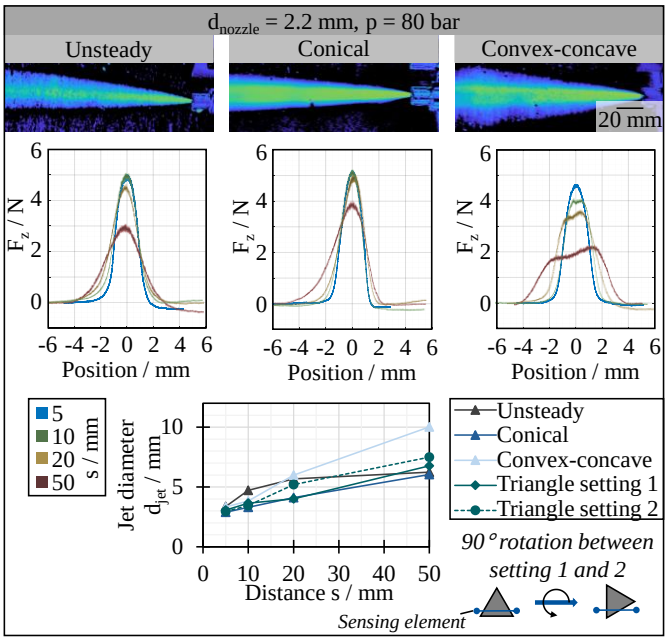

Fig. 14. Fluid free jet profiles for different round nozzles

Similar effects were visible for the rectangular nozzle (see Fig. 15). The jet energy distribution was not homogenous with a steady plateau along the outlet cross-section as would be expected and desired for this type of nozzle. Nevertheless, a rectangular nozzle geometry should be taken into account for the design of AM cutting tools as it allows a more focused cutting fluid supply along a wide range of the cutting edge compared to a circular outlet nozzle. A more regular jet profile might be generated with a longer outlet distance in the form of the final cross section, straightening the velocity vectors of the fluid.

As observed for the convex-concave and triangular nozzle, the jet energy for the L-formed nozzle was irregular and not uniform distributed along the axis of symmetry. The fluid density appeared higher in the outer areas of the free jet especially for higher outlet cross-sectional areas d_{nozzle} = 3 mm. As suggested for the rectangular nozzle profile, an increased outlet distance should be considered. The L-formed nozzle can

improve the focussed cutting fluid supply to the corner of the cutting edge. As in shoulder milling both the corner and the whole rake face of the cutting insert are strained, the nozzle geometry in the real cutting tool has to be modified according to the geometrical boundary conditions of the real application. Thus, the half symmetrical L-nozzle considered here has to be adapted and further investigated during the design process.

In general, the results indicate that for the design of AM cutting tools, the nozzle outlet should be positioned as close to the cutting edge and thus to the impingement point of the fluid free jet as possible to avoid jet expansion and an inhomogeneous fluid energy distribution. A small distance between outlet and cutting edge guarantees a focused cutting fluid supply with a maximum effect on lubrication and cooling.

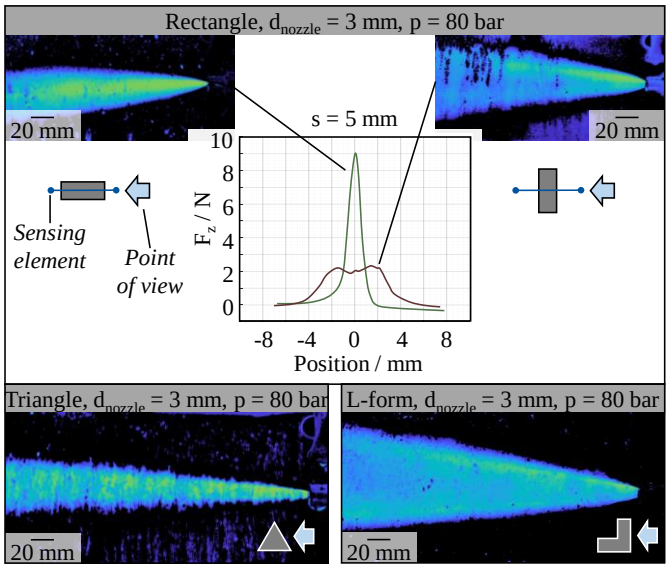

Fig. 15. Fluid free jet geometry for different non-rotational symmetric nozzle types

4. Conclusion and outlook

The results presented in this paper help to give design information for the construction of AM cutting tools. Some critical boundary conditions and limitations of additively manufactured coolant channels and outlet nozzles for the high-pressure cutting fluid supply were identified:

- At intersections between coolant channels, a transition radius should be implemented to reduce flow losses caused by turbulences after the directional change. A bigger radius does not necessarily lead to lower losses, which is important especially in constricted space conditions within a cutting tool. The surface roughness gains importance especially for channel diameters smaller than 2.2 mm as the percentage of the overflowed surface gets bigger.
- A triangular channel cross-section can improve surface roughness and geometrical accuracy compared to a circular coolant channel.
- Post-processing the inner channel surfaces can significantly reduce fluid friction. Thus, more fluid energy reaches the cutting zone. However, the material removal can cause an expansion of the cross-section. Consequently, parameters for abrasive flow machining have to be chosen carefully.
- In contrast to an unsteady and a convex-concave round nozzle, a conical nozzle geometry generates a homogenous and symmetrical fluid free jet allowing a focused fluid supply. The free jet generates high impact forces especially at low distances between outlet and impingement.
- Rectangular, L-shaped or other nozzle designs can help to form and focus the free jet depending on the application. However, powder adhesions and surface roughness prevent an exact prediction of the free jet geometry. The jet expansion at low distances is relatively constant for distances up to 10 mm.

Based on these results, further investigations regarding post-processing as well as outlet nozzle design will be conducted. First, the LPBF-process parameters have to be optimized regarding geometrical accuracy and surface roughness. The surface roughness depending on the build-up direction and orientation of the channel will be analysed. Abrasive flow machining will be performed in channel and nozzle test specimens with a lower material removal rate to only flatten the roughness peaks while maintaining the initial geometrical measures. Nozzles specifically designed for the application within AM indexable milling tools will be designed, analysed in CFD simulations and tested within the present boundary conditions set by the tool geometry and ideal impingement point of the cutting fluid in the cutting zone.

Acknowledgements

The IGF-research project 21049 N (Acronym: “TaCoMA”) of the Forschungsgemeinschaft Werkzeuge und Werkstoffe e.V. (FGW) is funded by the AiF within the program to promote joint industrial research (IGF) by the Federal Ministry for Economic Affairs and Energy, following a decision of the German Bundestag.

The LPBF manufactured parts within the research project were provided by the Fraunhofer Institute for Laser Technology (ILT) in Aachen, Germany with kind support from Jasmin Saewe. The authors would like to thank the companies Deutsche Edelstahlwerke Specialty Steel GmbH & Co. KG, 4 MI GmbH, LNS Group and Blaser Swisslube AG for the provision of material, service and cutting fluid.

References

[1] Klocke, F.; Döbbeler, B.; Lung, D. Energy Saving Potentials of High Pressure Lubricoolant Supply. Procedia CIRP, 2015, Vol. 26, p. 355–360
[2] Kovacevic, R.; Cherukuthota, C.; Mazurkiewicz, M. High Pressure Waterjet Cooling/Lubrication Improve Machining Efficiency In Milling. International Journal of Machine Tools and Manufacture, 1995, Vol. 35, No. 10, p. 1459–1473
[3] Klocke, F.; Sangermann, H.; Krämer, A.; Lung, D. Influence of a High-Pressure Lubricoolant Supply on Thermo-Mechanical Tool Load and Tool Wear Behaviour in the Turning of Aerospace Materials. Proceedings of the Institution of Mechanical Engineers, Part B: Journal of Engineering Manufacture, 2011, Vol. 225, No. 1, p. 52–61
[4] Ezugwu, E. O.; Bonney, J. Effect of high-pressure coolant supply when machining nickel-base, Inconel 718, alloy with coated carbide tools. Journal of Materials Processing Technology, 2004, Vol. 153-154, p. 1045–1050
[5] Ezugwu, E. O.; Bonney, J. Finish Machining of Nickel-Base Inconel 718 Alloy with Coated Carbide Tool under Conventional and High-Pressure Coolant Supplies. Tribology Transactions, 2005, Vol. 48, No. 1, p. 76–81
[6] Sangermann, H. Hochdruck-Kühlschmierstoffzufuhr in der Zerspanung. Dissertation. Aachen, 2013
[7] Klocke, F.; Döbbeler, B.; Lakner, T. Influence of cooling nozzle orientation on the machinability of TiAl6V4 and 42CrMo4+QT in rough milling. Procedia CIRP, 2018, Vol. 77, p. 66–69

[8] Klocke, F.; Dierckmann, J.; Garzón, M.; Kamenzky, S. Adaptation Of Cutting Tools By Eroding Miscellaneous Purging Ducts And Nozzles. International Conference on High Speed Machining, 2010, Vol. 8, p. 374–378
[9] Loichinger, A. Analyse und Optimierung der Kühlschmierstoff-Versorgung von rotierenden Werkzeugen. Dissertation. Dortmund, 2004
[10] Lakner, T.; Bergs, T.; Döbbeler, B. Additively manufactured milling tool with focused cutting fluid supply. Procedia CIRP, 2019, Vol. 81, p. 464–469
[11] Jahan, S. A.; El-Mounayri, H. Optimal Conformal Cooling Channels in 3D Printed Dies for Plastic Injection Molding. Procedia Manufacturing, 2016, Vol. 5, p. 888–900
[12] Klingaa, C. G.; Dahmen, T.; Baier, S.; Mohanty, S.; Hattel, J. H. X-ray CT and image analysis methodology for local roughness characterization in cooling channels made by metal additive manufacturing. Additive Manufacturing, 2020, Vol. 32, p. 101032
[13] Snyder, J. C.; Stimpson, C. K.; Thole, K. A.; Mongillo, D. Build Direction Effects on Additively Manufactured Channels. Journal of Turbomachinery, 2016, Vol. 138, No. 5
[14] Snyder, J. C.; Thole, K. A. Effect of Additive Manufacturing Process Parameters on Turbine Cooling. Journal of Turbomachinery, 2020, Vol. 142, No. 5
[15] Wildgoose, A. J.; Thole, K. A.; Sanders, P.; Wang, L. Impact of Additive Manufacturing on Internal Cooling Channels With Varying Diameters and Build Directions. Journal of Turbomachinery, 2021, Vol. 143, No. 7
[16] Morel, T. Comprehensive Design of Axisymmetric Wind Tunnel Contractions. Journal of Fluids Engineering, 1975, Vol. 97, No. 2, p. 225–233
[17] Morel, T. Design of Two-Dimensional Wind Tunnel Contractions. Journal of Fluids Engineering, 1977, Vol. 99, No. 2, p. 371–377
[18] Beer, N.; Özkaya, E.; Biermann, D. Drilling of Inconel 718 with Geometry-modified Twist Drills. Procedia CIRP, 2014, Vol. 24, p. 49–55
[19] Kalitzin, G.; Medic, G.; Iaccarino, G.; Durbin, P. Near-wall behavior of RANS turbulence models and implications for wall functions. Journal of Computational Physics, 2005, Vol. 204, No. 1, p. 265–291
[20] Schröder, W. Fluidmechanik. Reihe: Aachener Beiträge zur Strömungsmechanik, 7. Aufl. Aachen: Mainz, 2004
[21] Wulf, C. Geometrie und zeitliche Entwicklung des Schnittspaltes beim Wasserstrahlschneiden. Dissertation. Aachen, 1986
[22] Tenbrock, C.; Kelliger, T.; Praetzsch, N.; Ronge, M.; Jauer, L.; Schleifenbaum, J. H. Effect of laser-plume interaction on part quality in multi-scanner Laser Powder Bed Fusion. Additive Manufacturing, 2021, Vol. 38, p. 101810